

# VHE Gamma-Ray Induced Pair Cascades in Blazars and Radio Galaxies: Application to NGC 1275

P. Roustazadeh and M. Böttcher<sup>1</sup>

## ABSTRACT

Recent blazar detections by HESS, MAGIC, and VERITAS suggest that very-high-energy (VHE,  $E > 100$  GeV)  $\gamma$ -rays may be produced in most, if not all, types of blazars, including those that possess intense circumnuclear radiation fields. In this paper, we investigate the interaction of nuclear VHE  $\gamma$ -rays with the circumnuclear radiation fields through  $\gamma\gamma$  absorption and pair production, and the subsequent Compton-supported pair cascades. We have developed a Monte-Carlo code to follow the spatial development of the cascade in full 3-dimensional geometry, and calculate the radiative output due to the cascade as a function of viewing angle with respect to the primary VHE  $\gamma$ -ray beam (presumably the jet axis of the blazar). We show that even for relatively weak magnetic fields, the cascades can be efficiently isotropized, leading to substantial off-axis cascade emission peaking in the *Fermi* energy range at detectable levels for nearby radio galaxies. We demonstrate that this scenario can explain the *Fermi* flux and spectrum of the radio galaxy NGC 1275.

*Subject headings:* galaxies: active — gamma-rays: theory — radiation mechanisms: non-thermal

## 1. Introduction

Blazars, a class of active galactic nuclei (AGNs) comprised of Flat-Spectrum Radio Quasars (FSRQs) and BL Lac objects, exhibit some of the most violent high-energy phenomena observed in AGNs to date. Their spectral energy distributions (SEDs) are characterized by non-thermal continuum spectra with a broad low-frequency component in the radio –

---

<sup>1</sup>Astrophysical Institute, Department of Physics and Astronomy, Ohio University, Athens, OH 45701, USA

UV or X-ray frequency range and a high-frequency component from X-rays to  $\gamma$ -rays. They show rapid variability across the electromagnetic spectrum. In extreme cases, the very-high-energy (VHE)  $\gamma$ -ray emission of blazars has been observed to vary on time scales of just a few minutes (Albert et al. 2007a; Aharonian et al. 2007).

Leptonic and hadronic models (for a recent review see, e.g. Böttcher 2007) can generally successfully account for the overall SEDs observed from the known VHE  $\gamma$ -ray blazars, which are almost all BL Lac objects. BL Lac objects span a wide range of synchrotron peak frequencies, from IR to X-rays. According to the location of the synchrotron peak, they are classified as Low frequency peaked BL Lacs (LBLs: synchrotron peak in the IR), intermediate BL Lac objects (IBLs: synchrotron peak in the optical/UV) or High frequency peaked BL Lacs (HBLs: synchrotron peak in the X-rays). Until very recently, all known VHE  $\gamma$ -ray blazars were HBLs. However, the recent detections of the IBLs W Comae, 3C 66A, and PKS 1424+240 by VERITAS (Acciari et al. 2008, 2009, 2010), the LBLs BL Lacertae and S5 0716+714 by MAGIC (Albert et al. 2007b; Anderhub et al. 2009), and even the Flat-Spectrum Radio Quasars (FSRQs) 3C 279 by MAGIC (Albert et al. 2008) and PKS 1510-089 by HESS (Wagner & Behera 2010) suggest that most blazars are intrinsically emitters of VHE  $\gamma$ -rays.

The fact that most LBLs and FSRQs have not been detected as VHE  $\gamma$ -ray sources might be primarily a result of the absorption of VHE  $\gamma$ -rays by lower-frequency (IR – optical – UV) radiation. As those objects tend to be located at greater cosmological distances ( $z \gtrsim 0.2$ ),  $\gamma\gamma$  absorption on the Extragalactic Background Light (EBL) becomes substantial, suppressing any intrinsically produced  $> 100$  GeV emission (e.g. Dwek & Krennrich 2005; Stecker & Scully 2008; Franceschini et al. 2008; Finke & Razzaque 2009; Finke et al. 2010). However, possibly even more importantly, multi-GeV  $\gamma$ -rays produced in the high-radiation-density environment within the broad line region (BLR) and the dust torus of a quasar, is expected to be strongly attenuated by  $\gamma\gamma$  pair production (e.g. Protheroe & Biermann 1997; Donea & Protheroe 2003; Reimer 2007; Liu et al. 2008; Sitarek & Bednarek 2008). The studies cited above show that for typical parameters expected in 3C279, photons above  $\sim 100$  GeV are expected to be strongly attenuated unless the  $\gamma$ -ray emission region is located beyond the broad line region. If VHE  $\gamma$ -rays are produced very close to the central engine, also  $\gamma\gamma$  absorption by the direct accretion disk emission may become substantial (Sitarek & Bednarek 2010).

Given the now substantial number of non-HBL VHE  $\gamma$ -ray blazars, it seems plausible that most LBLs and FSRQs and their misaligned parent population, radio galaxies, are producing VHE  $\gamma$ -ray emission within their blazar zone. This view is also supported by the detection of VHE  $\gamma$ -ray emission from two non-blazar AGNs, namely the radio galaxies

M87 (Aharonian et al. 2004) and Cen A (Aharonian et al. 2009). The non-detection of VHE  $\gamma$ -rays from most LBLs and FSRQs might then be due to the combined effects of local and intergalactic  $\gamma\gamma$  absorption. As a consequence of  $\gamma\gamma$  absorption in the local radiation field of the AGN, GeV – TeV electron-positron pairs are injected into the AGN environment, which, in the dense radiation field within the BLR and the dust torus of quasars, may initiate inverse-Compton supported pair cascades.

The development of pair cascades induced by VHE  $\gamma$ -ray emission from blazars has so far concentrated on the development of Mpc-scale pair halos resulting from the interaction of ( $\gtrsim 100$  TeV)  $\gamma$ -rays with the Cosmic Microwave background (e.g. Aharonian et al. 1994), or of VHE ( $\gtrsim 100$  GeV)  $\gamma$ -rays by the EBL (Venters 2010). Due to the long Compton cooling timescale of pairs on the CMB or the EBL, those authors could reasonably consider the produced cascades isotropic, leading to an extended pair halo around the AGN. Small-angle deflection of secondaries in weak intergalactic magnetic fields has been included in those considerations by Plaga (1995) and Elyiv et al. (2009). The development of pair cascades within the AGN has been discussed by Bednarek & Kirk (1995) and Sitarek & Bednarek (2010).

Depending on the magnetic field strength and orientation in the extended nuclear region, cascades developing within the high-radiation-energy-density environment within the BLR of a quasar may be efficiently isotropized in the immediate vicinity of the AGN. This will lead to distinct spectral features, which we will consider in this paper. In Section 2 we present some general considerations and analytic estimates of the expected results, including an estimate of the required magnetic field strengths within  $\sim$  a few pc from the central engine of a blazar (or radio galaxy), for which secondary electrons and positrons in pair cascades initiated by primary VHE  $\gamma$ -rays may be efficiently isotropized within the central region. The consequence would be quasi-isotropic radiation signatures from Compton-supported pair cascades, potentially observable in the *Fermi* energy range. In Section 3 we will describe a numerical code that treats the full three-dimensional development of these cascades, together with the general model setup and simplifying assumptions. Numerical results for generic parameters will be presented in Section 4. In Section 5, we will demonstrate that the recent *Fermi* detection of the radio galaxy NGC 1275 (Abdo et al. 2009a) can be plausibly explained by the cascade emission from a misaligned VHE  $\gamma$ -ray emitting blazar. We summarize and present an outlook towards future work in Section 6.

## 2. General Considerations and Estimates

In the limit of a VHE  $\gamma$ -ray photon with energy  $E_\gamma$  interacting with an IR/optical/UV photon from the dust torus or the BLR with energy  $E_s \ll E_\gamma$ , an electron-positron pair with particle energy  $E_e = \gamma m_e c^2 \approx E_\gamma/2 \equiv 1 E_{\text{TeV}}$  TeV will be produced, moving along the direction of the primary  $\gamma$ -ray photon to within an accuracy of  $\Delta\theta \sim 1/\gamma$ . Depending on the strength of the magnetic field near the point of pair production,  $B \equiv 1 B_{-6} \mu\text{G}$ , they will be deflected on a length scale of the order of the Larmor radius,

$$r_g \sim 10^{-3} E_{\text{TeV}} B_{-6}^{-1} \text{ pc}. \quad (1)$$

To investigate whether particles are efficiently isotropized before producing secondary synchrotron and/or inverse-Compton (IC) emission, the isotropization length has to be compared with the radiative cooling length,  $\lambda_{\text{sy}}$  and  $\lambda_{\text{IC}}$ , respectively. The synchrotron cooling length can be estimated to

$$\lambda_{\text{sy}} \sim 3.8 \times 10^6 E_{\text{TeV}}^{-1} B_{-6}^{-2} \text{ pc}. \quad (2)$$

To estimate the IC cooling length on an external radiation field from the BLR we calculate its energy density as  $u_{\text{BLR}} \sim L_D \tau_{\text{BLR}} / (4\pi R_{\text{BLR}}^2 c)$ , which we parameterize through the accretion disk luminosity  $L_D \equiv 10^{46} L_{46} \text{ erg s}^{-1}$  and a BLR with a reprocessing optical depth of  $\tau_{\text{BLR}} \equiv 0.1 \tau_{-1}$  at an average distance of  $R_{\text{BLR}} \equiv 0.1 R_{-1} \text{ pc}$  from the central engine. Hence, the total luminosity of the BLR will be  $L_{\text{BLR}} = \tau_{\text{BLR}} L_D$ . If Compton scattering occurs in the Thomson regime, we find

$$\lambda_{\text{IC}} \sim 5 \times 10^{-6} E_{\text{TeV}}^{-1} L_{46}^{-1} \tau_{-1}^{-1} R_{-1}^2 \text{ pc}. \quad (3)$$

This illustrates that one may expect particles at energies substantially below 1 TeV to be fully isotropized, while higher-energy particles might lose a substantial fraction of their energy while still traveling along the primary VHE  $\gamma$ -ray beam. Comparison of the synchrotron and IC cooling lengths suggests that the radiative output from the secondaries will be strongly dominated by IC emission, initiating an IC-supported cascade (e.g. Protheroe 1986; Zdziarski 1988). At low frequencies far below the pair production threshold, produced by secondaries which are fully isotropized (i.e.,  $\lambda_{\text{IC}} \gg r_g$ ), the cascade spectrum will obtain a  $\nu F_\nu \propto \nu^{1/2}$  shape. This is the consequence of the secondaries being injected at high energies and then being subject to Compton cooling in the Thomson regime, resulting in a  $N(\gamma) \propto \gamma^{-2}$  pair spectrum. This low-energy spectral shape (though not its total flux) will be independent of the primary gamma-ray spectrum. Two effects will produce a turnover towards higher frequencies. First, for any given viewing angle  $\theta$  with respect to the direction of propagation of the primary  $\gamma$ -ray (being absorbed in the  $\gamma\gamma$  pair production process), we can find a critical electron energy for which the deflection angle over a Compton length equals the observing

angle, i.e.,  $\theta \sim \lambda_{\text{IC}}/r_g$ . Higher-energy particles will radiate preferentially at smaller viewing angles, while lower-energy particles can efficiently contribute to the emission at the given angle. This yields the characteristic electron energy  $E_{e,\text{br}}$  corresponding to a given observing angle  $\theta$ :

$$E_{e,\text{br}} = m_e c^2 \sqrt{\frac{3 e B}{4 \sigma_T u_{\text{BLR}} \theta}} \sim 70 B_{-6}^{1/2} R_{-1} L_{46}^{-1/2} \tau_{-1}^{-1/2} \theta^{-1/2} \text{ GeV}. \quad (4)$$

If these electrons can scatter the soft photon field in the Thomson regime, a turnover should occur at photon energies of

$$E_{\text{IC,br}} = \frac{3 e B}{4 \sigma_T u_{\text{BLR}} \theta} E_s \sim 18 B_{-6} R_{-1}^2 L_{46}^{-1} \tau_{-1}^{-1} \theta^{-1} \left( \frac{E_s}{\text{eV}} \right) \text{ GeV}. \quad (5)$$

We point out that, in this estimate, we assumed that the Compton cooling length is a realistic measure of the distance travelled by the electron/positron since its production from annihilation of a primary  $\gamma$ -ray. This approximation will break down if the particles require multiple Compton scatterings to reach the break energy corresponding to Eq. 5. This is due to both an increasing Compton cooling length and a decreasing Larmor radius as the electron energy is reduced by previous scatterings.

Second, if Compton scattering to energies given by Eq. 5 occurs in the Klein-Nishina regime (which is the case if  $E_{\text{IC,br}} \geq E_{e,\text{br}}$ ) a turnover is expected at the transition from Thomson to Klein-Nishina scattering at

$$E_{\text{IC,KN}} = 260 \left( \frac{E_s}{\text{eV}} \right)^{-1} \text{ GeV}. \quad (6)$$

### 3. Model Setup and Code Description

The geometrical setup of our model system is illustrated in Figure 1. The primary VHE  $\gamma$ -ray emission from the blazar zone is represented as a mono-directional beam of  $\gamma$ -rays propagating along the X axis. The incident VHE  $\gamma$ -ray spectrum is represented by a straight power-law with photon index  $\alpha$ . Those  $\gamma$ -rays may interact via  $\gamma\gamma$  absorption and pair production with a radiation field. For a first general investigation and feasibility study presented here, we approximate the radiation field as monoenergetic and isotropic within a fixed boundary, given by a radius  $R_{\text{ext}}$ , i.e.,

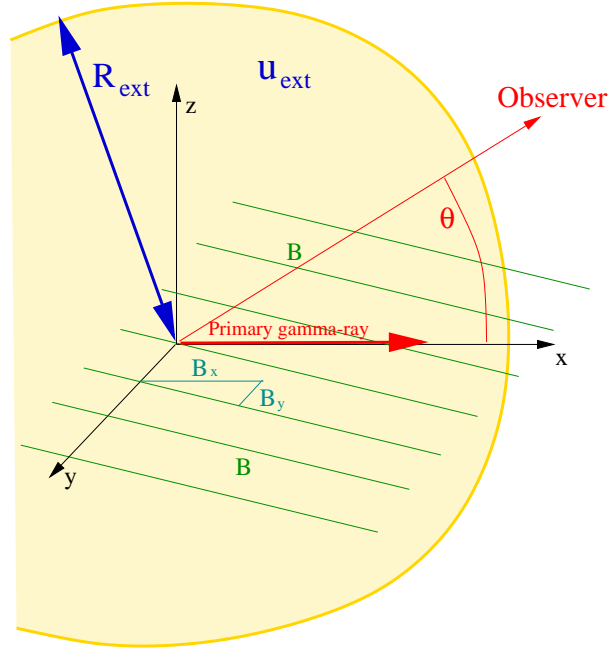


Fig. 1.— Geometry of the model setup.

$$u_{\text{ext}}(\epsilon, r, \Omega) = u_0 \delta(\epsilon - \epsilon_{\text{ext}}) H(R_{\text{ext}} - r) \quad (7)$$

where  $H$  is the Heaviside function,  $H(x) = 1$  if  $x > 0$  and  $H(x) = 0$  otherwise. A magnetic field of order  $\sim \mu\text{G}$  is present. Without loss of generality, we choose the  $y$  and  $z$  axes of our coordinate system such that the magnetic field lies in the  $(x,y)$  plane.

We have developed a Monte-Carlo code which treats the processes of  $\gamma\gamma$  absorption and pair production,  $\gamma$ -ray and electron/positron propagation, and Compton scattering. The code generates a single  $\gamma$ -ray photon at a time, at the origin of our coordinate system, propagating in the  $x$  direction. In order to improve the statistics of the otherwise very few highest-energy photons, we introduce a statistical weight inversely proportional to the photon energy. The code calculates the absorption opacity  $\kappa_{\gamma\gamma}$ , using the full pair production cross section. Based on the corresponding absorption length, a location for the occurrence of the next  $\gamma\gamma$  absorption / pair production process is drawn. If the pair production site is outside the radius  $R_{\text{ext}}$ , the photon escapes; otherwise, the photon is absorbed, and an electron-positron pair is created. The code uses the analytic result for the  $\gamma\gamma$  pair production spectrum of Böttcher & Schlickeiser (1997) to draw the energies of the electron and the positron. As motivated above, we assume that both particles initially propagate in the direction of the absorbed  $\gamma$ -ray. For both particles, the Compton scattering length  $\lambda_{\text{IC}}$  is

calculated using the full Compton cross section. As we expect the magnetic-field energy density to be much smaller than the radiation energy density, we neglect synchrotron losses to the electrons/positrons. Based on the value of  $\lambda_{\text{IC}}$ , the code draws a length that the electron/positron travels before the next Compton scattering event occurs. It then propagates the electron/positron, using the full 3-D geometry, through its gyrotational motion in the magnetic field, to calculate the (x,y,z) coordinates and direction of motion of the electron/positron at the point of scattering. If this point of scattering is outside the radius  $R_{\text{ext}}$ , the electron/positron escapes; otherwise, Compton scattering occurs. The energy of the produced photon is drawn using a  $\delta(\Omega_{\text{sc}} - \Omega_e)$  approximation for the Compton cross section (e.g., Dermer & Böttcher 2006), i.e., the scattered photon is traveling in the same direction as the electron/positron before scattering. The produced ( $\gamma$ -ray) photon is then tracked through the same photon tracking routine as the primary VHE  $\gamma$ -ray photons (properly accounting for the correct location and direction of propagation). The energy of the electron/positron is reduced by the energy of the scattered photon, and the particle is returned to the pair tracking routine. If the energy of the electron/positron is below a set threshold (determined by the condition that they will no longer produce Compton emission in the energy range of interest), the code will move on to the next particle.

The energies, statistical weights, and directions of propagation of photons escaping from the region of high external radiation field (bounded by  $R_{\text{ext}}$ ), are written into a photon event file. In a post-processing routine, this event file will be read to produce photon spectra with arbitrary energy and angular binning.

#### 4. Numerical Results

We have used the cascade Monte-Carlo code described in the previous section to evaluate the angle-dependent cascade spectra for a variety of generic parameter choices. Figure 2 illustrates the viewing angle dependence of the cascade emission. For this simulation, we assumed a magnetic field of  $B = 1 \mu\text{G}$ , oriented at an angle  $\theta_B = 5.7^\circ$  with respect to the X axis ( $B_x = 1 \mu\text{G}$ ,  $B_y = 0.1 \mu\text{G}$ ). The external radiation energy density is  $u_0 = 10^{-2} \text{ erg cm}^{-3}$ , extended over a region of radius  $R_{\text{ext}} = 10^{19} \text{ cm}$  with photon energy  $E_s = E_{\text{Ly}\alpha}$ . The incident  $\gamma$ -ray spectrum has a photon index of  $\alpha = 2.5$  and extends out to  $E_{\gamma,\text{max}} = 5 \text{ TeV}$ . The results have been normalized to a flux level in the forward direction corresponding to a  $\gamma$ -ray bright blazar. The spectra for all other directions have been normalized with the same normalization factor. The curves are labeled by the cosine of the observing angle,  $\mu = \cos \theta_{\text{obs}}$ . In the forward (blazar) direction, one clearly sees the  $\gamma\gamma$  absorption cut-off at an energy  $E_c = (m_e c^2)^2 / E_s \sim 25 \text{ GeV}$ . The cutoff is very sharp in this simulation because of

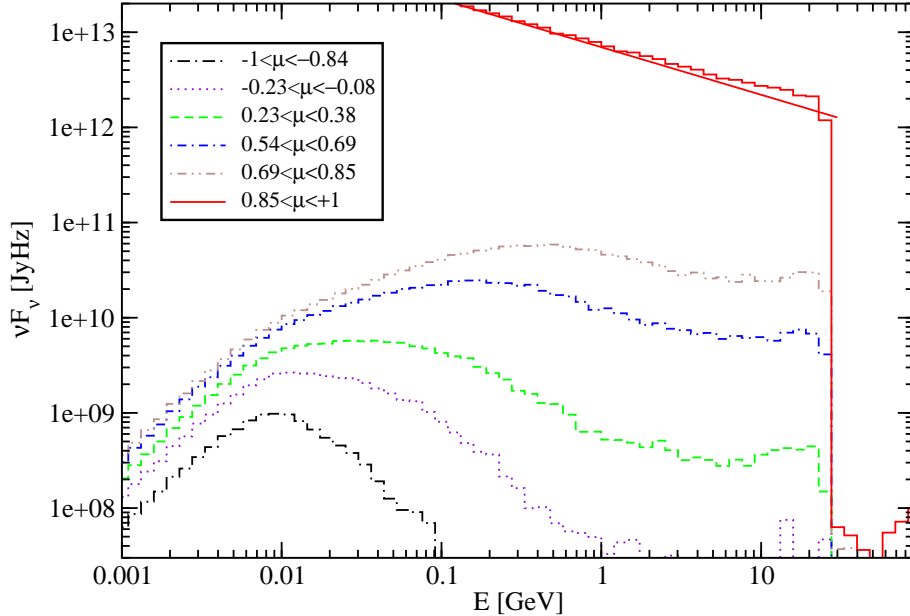


Fig. 2.— Cascade emission at different viewing angles ( $\mu = \cos \theta_{\text{obs}}$ ). Parameters:  $B = 1 \mu\text{G}$ ,  $\theta_B = 5.7^\circ$ ;  $u_0 = 10^{-2} \text{ erg cm}^{-3}$ ,  $R_{\text{ext}} = 10^{19} \text{ cm}$ ,  $E_s = E_{\text{Ly}\alpha}$ ,  $\alpha = 2.5$ ,  $E_{\gamma, \text{max}} = 5 \text{ TeV}$ . The solid (red) straight line indicates the incident primary  $\gamma$ -ray spectrum.

our  $\delta$  approximation of the external radiation field, combined with a high  $\gamma\gamma$  absorption depth near threshold for the parameters chosen here. Below this cutoff, the forward-component of the cascade emission leads to a slight bump beyond the primary  $\gamma$ -ray power-law spectrum. The cascade emission at larger viewing angles  $\mu < 0.85$  has a low-frequency shape close to the expected  $\nu F_\nu \propto \nu^{1/2}$  behaviour, and exhibits the progressive suppression of the cascade emission at high energies with increasing viewing angle due to incomplete isotropization of the secondary particles at high energies, as expected from Eq. 5.

Figure 3 illustrates the effect of a varying external radiation field energy density  $u_0$ . For energy densities  $u_0 \gtrsim 10^{-3} \text{ erg cm}^{-3}$ ,  $\gamma\gamma$  absorption is essentially saturated, i.e., all VHE photons above the pair production threshold will be absorbed. Hence, the magnitude of the cascade becomes almost independent of  $u_0$ . For smaller  $u_0$ , the decreasing flux in the cascade emission reflects the decreasing fraction of VHE  $\gamma$ -ray photons absorbed. This latter is the regime in which our estimate of the turnover frequency (Eq. 5) is applicable. In the saturated regime, the electrons/positrons have to undergo many scatterings before reaching the isotropization energy so that the Compton scattering length is no longer an appropriate measure of the distance traveled, as assumed in the derivation of Eq. 5. As expected, the low  $u_0$  case results in a larger turnover energy than the high  $u_0$  cases.

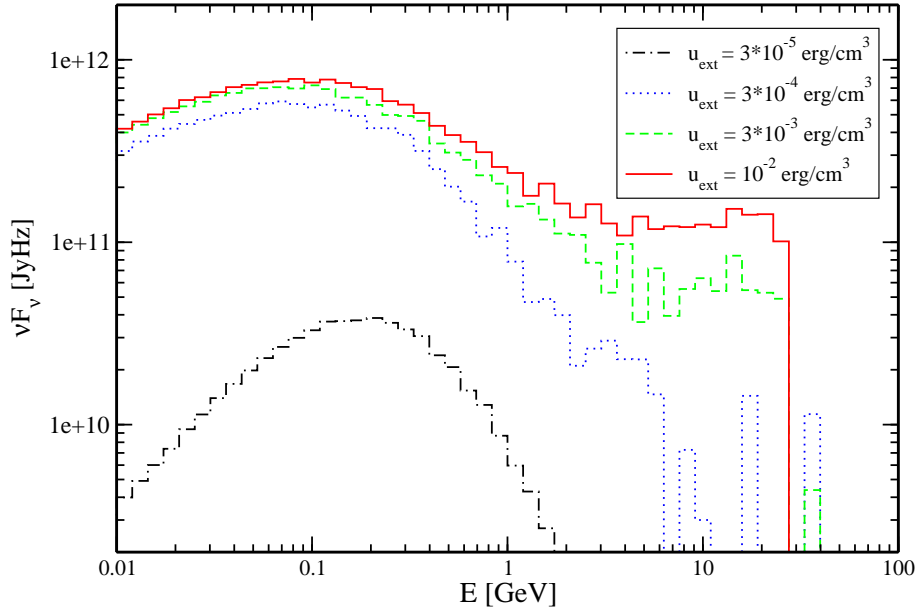


Fig. 3.— The effect of a varying external radiation energy density. Parameters are the same as for Figure 2 in the angular bin  $0.38 \leq \mu \leq 0.54$ .

The effect of a varying magnetic field strength for fixed magnetic field orientation ( $\theta_B = 45^\circ$ ) is illustrated in Figure 4. We see that the cascade development is extremely sensitive to the transverse magnetic field  $B_y$  for weak magnetic fields. The cascades exhibit a rapid transition to the limit in which even the highest-energy secondary particles are effectively isotropized before undergoing the first Compton scattering interaction. Hence, for magnetic field values expected on sub-pc or pc scales around an AGN ( $B \gg 1$  nG) and large angles  $\theta_B$ , there is no pronounced break in the cascade spectrum out to large energies near the  $\gamma\gamma$  absorption trough at  $E_c$ .

Figure 5 shows the effect of a varying magnetic-field orientation with respect to the jet axis, for fixed magnetic-field strength  $B = 1 \mu\text{G}$ . The figure illustrates that it is primarily the perpendicular ( $B_y$ ) component of the magnetic field which is responsible for the isotropization of secondaries in the cascade. Obviously, for a perfectly aligned magnetic field ( $\theta_B = 0^\circ$ ), our code does not predict any cascade emission in any off-axis direction, since we neglect the spreading of the cascade due to the kinematics of the pair-production process or recoil from Compton scattering. For a small inclination angle, the small perpendicular magnetic-field component leads to inefficient isotropization and, hence, a break in the off-axis cascade spectrum at low energies. For large inclination angles ( $B_y \gtrsim B_x$ ), isotropization becomes very efficient out to energies close to the  $\gamma\gamma$  absorption trough.

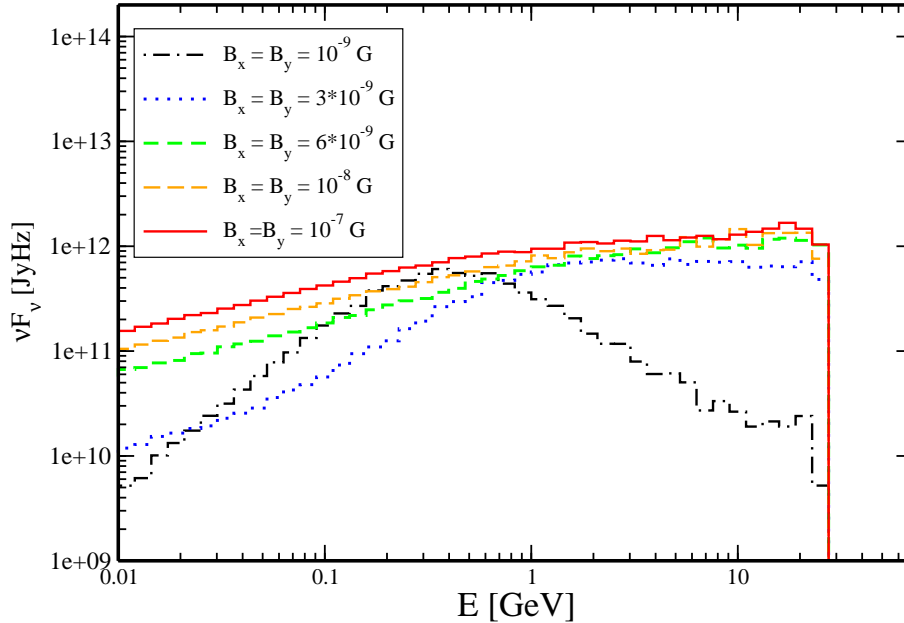


Fig. 4.— The effect of a varying magnetic field strength, for a fixed angle of  $\theta_B = 45^\circ$  between jet axis and magnetic field. All other parameters are the same as for Figure 2 in the angular bin  $0.38 \leq \mu \leq 0.54$ .

## 5. Application to Radio galaxies: The case of NGC 1275

From the numerical results shown above it has become obvious that VHE  $\gamma$ -ray induced cascades even in the presence of rather weak ( $\sim \mu\text{G}$ ) magnetic fields can be efficiently isotropized and produce a substantial MeV – GeV  $\gamma$ -ray flux in directions misaligned with respect to the jet axis (the forward or “blazar” direction). The standard AGN unification scheme (Urry & Padovani 1995) proposes that blazars and radio galaxies are intrinsically identical objects viewed at different angles with respect to the jet axis. According to this scheme, FR I and FR II radio galaxies are believed to be the parent population of BL Lac objects and FSRQs, respectively. Hence, if most blazars, including LBLs and FSRQs, are intrinsically VHE  $\gamma$ -ray emitters potentially producing pair cascades in their immediate environments, the radiative signatures of these cascades might be observable in many radio galaxies. In fact, already three radio galaxies (NGC 1275: Abdo et al. (2009a), M 87: Abdo et al. (2009b), and Cen A: Abdo et al. (2009c)) have been detected by Fermi, while *EGRET* provided evidence for  $> 100$  MeV  $\gamma$ -ray emission from two more radio galaxies, 3C 111 (Nandikotkur et al. 2007) and NGC 6251 (Mukherjee et al. 2002). In this paper, we focus on the radio galaxy NGC 1275 (Abdo et al. 2009a) and investigate whether the Fermi

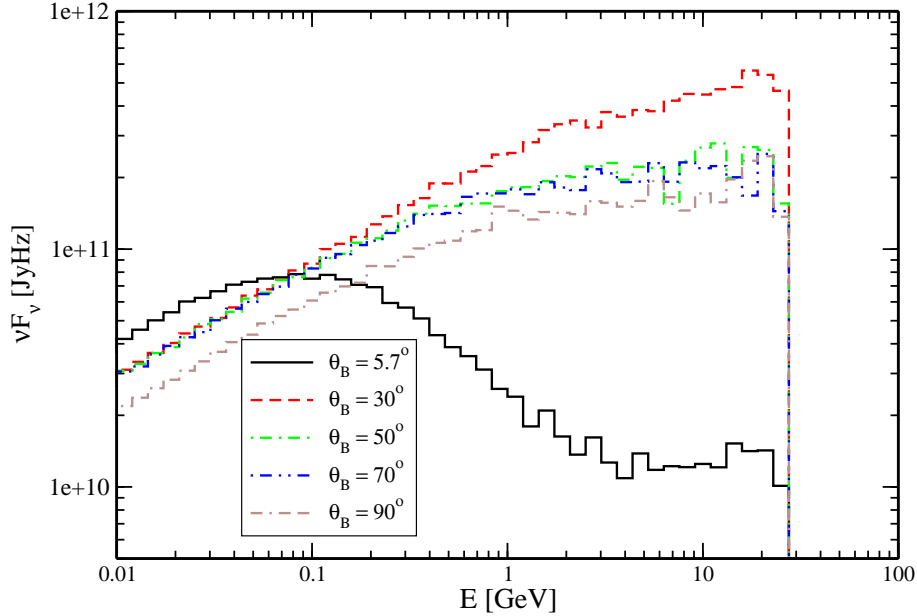


Fig. 5.— The effect of a varying magnetic field orientation, for a fixed magnetic field strength of  $B = 1 \mu\text{G}$ . All other parameters are the same as for Figure 2 in the angular bin  $0.38 \leq \mu \leq 0.54$ .

spectrum and flux level are consistent with the interpretation of cascade emission from a misaligned,  $\gamma\gamma$  absorbed blazar.

NGC 1275 is located at a distance of  $d = 74$  Mpc. It hosts the powerful FR I radio galaxy Perseus A (= 3C 84). The radio jet is directed at an angle of  $\theta \approx 30^\circ - 55^\circ$  with respect to the line of sight (Walker et al. 1994). NGC 1275 also hosts a Seyfert-like nucleus with a total line luminosity of  $L_{\text{BLR}} = 1.6 \times 10^{42} \text{ erg s}^{-1}$  (Zirbel & Baum 1995). Fermi observed a  $\gamma$ -ray flux of  $F(> 100 \text{ MeV}) = (2.10 \pm 0.23) \times 10^{-8} \text{ ph cm}^{-2} \text{ s}^{-1}$  from NGC 1275, which could be fit by a power-law with a photon index of  $\Gamma = 2.17 \pm 0.05$  (Abdo et al. 2009a). However, the Fermi spectrum does seem to exhibit a marked steepening towards higher energies. A comparison with the EGRET upper limit indicates substantial flux variability on time scales of years to decades, indicating that the  $\gamma$ -ray emission must be produced in a region of  $R \lesssim$  a few pc.

Our simulation results can be properly normalized to the expected flux for a radio galaxy with the following considerations: The forward spectrum shown in Figure 2 corresponds to the escaping radiation in a solid angle interval  $\Delta\Omega = 2\pi \Delta\mu$ , where  $\Delta\mu = 0.15$  in the examples shown here. However, the cone of blazar emission might be smaller, namely  $\Delta\Omega_b \approx \pi\theta_b^2$ , where  $\theta_b$  is the opening angle of the blazar emission cone. Hence, a realistic flux

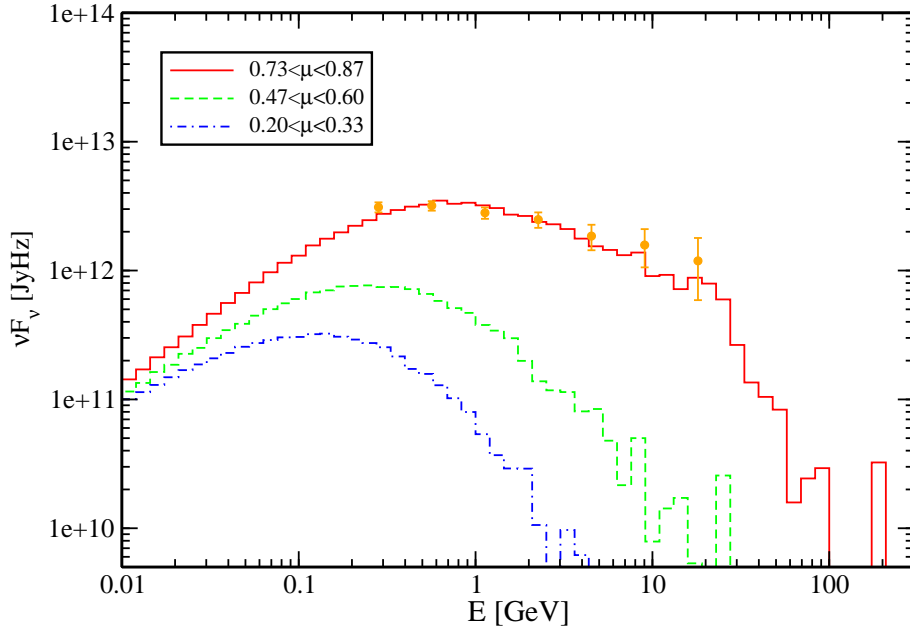


Fig. 6.— Fit to the *Fermi* spectrum of NGC 1275 with a simulated cascade spectrum from a mis-aligned blazar, along with the cascade spectra at larger viewing angles.

normalization for any off-axis direction requires a correction factor of  $f_{\text{ang}} = \theta_b^2 / (2 \Delta\mu)$ . The normalization will also depend on the difference in distances,  $f_{\text{dist}} = (d_{\text{bl}}/d_{\text{RG}})^2$ , where  $d_{\text{bl}}$  and  $d_{\text{RG}}$  are the luminosity distances of the blazar and the radio galaxy, respectively. Hence, we apply a total normalization factor  $f = f_{\text{ang}} f_{\text{dist}}$ .

Figure 6 illustrates that the Fermi spectrum of NGC 1275 can be well matched with a VHE  $\gamma$ -ray induced cascade from a misaligned blazar. For the normalization of the incident  $\gamma$ -ray beam, we used the Fermi spectrum of the blazar 3C279 at  $d_L = 2.2$  Gpc. The external radiation field is parameterized through  $u_{\text{ext}} = 5 \times 10^{-2}$  erg cm $^{-3}$  and  $R_{\text{ext}} = 10^{16}$  cm. This size scale is appropriate for low-luminosity AGN as observed in NGC 1275 (e.g. Kaspi et al. 2007), and the parameters combine to a BLR luminosity of  $L_{\text{BLR}} = 4\pi R_{\text{ext}}^2 c u_{\text{ext}} = 1.9 \times 10^{42}$  erg s $^{-1}$ , in agreement with the observed value for NGC 1275. The magnetic field is  $B = 1$  mG, oriented at an angle of  $\theta_B = 8^\circ$ . The cascade spectrum shown in Figure 6 pertains to the angular bin  $0.73 < \mu < 0.87$  (corresponding to  $30^\circ \lesssim \theta \lesssim 43^\circ$ ), appropriate for the known orientation of NGC 1275. The factor required to re-normalize between the simulated spectrum in the forward direction (at a flux level observed for 3C 279) and the sideways spectrum, fit to NGC 1275, was  $f = f_{\text{ang}} f_{\text{dist}} = 146$ . This corresponds to a blazar cone opening angle of  $\theta_b = 12.7^\circ$  for 3C279. It should be pointed out that our normalization to flux levels of 3C279 are only meant to demonstrate that our parameter values correspond

to conditions reasonably expected in misaligned blazars in general. The numbers quoted above pertaining to 3C 279 should not be taken at face value as a diagnostic for 3C279 itself.

## 6. Summary and Outlook

We have developed a Monte-Carlo code to simulate the full 3-D development of VHE  $\gamma$ -ray induced pair cascades in the weakly magnetized environments of blazars and radio galaxies. These cascades develop as Compton-supported pair cascades if there is a substantial radiation energy density, e.g., from the broad-line region or the dust torus around the central engine. We have demonstrated the angle-dependence of these cascades as a function of the magnetic field and the radiation energy density in the AGN environment. In the off-axis directions, these cascades exhibit a  $\nu F_\nu \propto \nu^{1/2}$  spectrum at low energies and a turnover towards higher energies due to incomplete isotropization of high-energy secondaries in the cascade, depending on the strength and orientation of the magnetic field and the radiation energy density.

We have demonstrated that the off-axis cascade emission may well be detectable from nearby radio galaxies, which, according to the blazar unification scheme, are the mis-aligned parent population of blazars. We have presented a fit to the *Fermi* spectrum of the radio galaxy NGC 1275 with parameters expected if this radio galaxy is the mis-aligned counterpart of a typical *Fermi*-detected blazar.

The present work is to be understood as a general proof of the potential importance of VHE  $\gamma$ -ray induced pair cascades in blazar environments. For this purpose, we have used a simplified representation of the radiation field as monoenergetic, homogeneous and isotropic out to a limiting radius. In future work, we will relax this assumption to allow for an arbitrary radiation spectrum and more realistic spatial and angular dependence. While we expect slight quantitative differences in the spectral shape of the emanating cascade emission due to these modifications, the general viability of the process as well as its dependence on magnetic field properties and the external radiation field are expected to remain robust predictions of our work.

We thank Jun Kataoka for sending us the Fermi data points for NGC 1275. This work was supported by NASA through Fermi Guest Investigator Grant NNX09AT81G.

## REFERENCES

- Abdo, A. A., et al., 2009a, *ApJ*, 699, 31
- Abdo, A. A., et al., 2009b, *ApJ*, 707, 55
- Abdo, A. A., et al., 2009c, *ApJ*, 700, 597
- Acciari, V. A., et al., 2008, *ApJ*, 684, L73
- Acciari, V. A., et al., 2009, *ApJ*, 693, L104
- Acciari, V. A., et al., 2010, *ApJ*, 708, L100
- Aharonian, F. A., Coppi, P. S., & Völk, H. J., 1994, *ApJ*, 423, L5
- Aharonian, F., et al., 2004, *A&A*, 421, 529
- Aharonian, F., et al., 2007, *ApJ*, 664, L71
- Aharonian, F., et al., 2009, *Apj*, 695, L40
- Albert, J., et al., 2007a, *ApJ*, 669, 862
- Albert, J., et al., 2007b, *ApJ*, 666, L17
- Albert, J., et al., 2008, *Science*, 320, 1752
- Anderhub, H., et al., 2009, *ApJ*, 704, L129
- Bednarek, W., & Kirk, J. G., 1995, *A&A*, 294, 366
- Böttcher, M., & Schlickeiser, R., 1997, *A&A*, 325, 866
- Böttcher, M., 2007a, in proc. “The Multimessenger Approach to Gamma-Ray Sources”, *ApSS*, 309, 95
- Dermer, C. D., & Böttcher, M., 2006, *ApJ*, 643, 1081
- Donea, A. C., & Protheroe, R. J., 2003, *Astrop. Phys.*, 18, 337
- Dwek, E., & Krennrich, F., 2005, *ApJ*, 618, 657
- Elyiv, A., Neronov, A., & Semikoz, D. V., 2009, *Phys. Rev. D*, 80, 2, 023010
- Finke, J. D., & Razzaque, S., 2009, *ApJ*, 698, 1761

- Finke, J. D., Razzaque, S., & Dermer, C. D., 2010, *ApJ*, 712, 238
- Franceschini, A., Rodighiero, G., & Vaccari, M., 2008, *A&A*, 487, 837
- Kaspi, S., Brandt, W. N., Maoz, D., Netzer, H., Schneider, D. P., & Shemmer, O., 2007, *ApJ*, 659, 997
- Liu, H. T., Bai, J. M., & Ma, L., 2008, *ApJ*, 688, 148
- Mukherjee, R., Halpern, J., Mirabal, N., & Gotthelf, E. V., 2002, *ApJ*, 574, 693
- Nandikotkur, G., et al., 2007, *ApJ*, 657, 706
- Plaga, R., 1995, *Nature*, 6521, 430
- Protheroe, R. J., 1986, *MNRAS*, 221, 769
- Protheroe, R. J., & Biermann, P. L., 1997, *Astrop. Phys.*, 6, 293
- Reimer, A., 2007, *ApJ*, 665, 1023
- Sitarek, J., & Bednarek, W., 2008, *MNRAS*, 391, 624
- Sitarek, J., & Bednarek, W., 2010, *MNRAS*, 401, 1983
- Stecker, F. W., & Scully, S. T., 2008, *A&A*, 478, L1
- Urry, C. M., & Padovani, P., 1995, *PASP*, 107, 803
- Wagner, S., & Behera, B., 2010, 10<sup>th</sup> HEAD Meeting, Hawaii (BAAS, 42, 2, 07.05)
- Walker, R. C., Romney, J. D., & Benson, J. M., 1994, *ApJ*, 430, L45
- Venters, T. M., 2010, *ApJ*, 710, 1530
- Zdziarski, A. A., 1988, *ApJ*, 335, 786
- Zirbel, E. L., & Baum, S. ., 1995, *ApJ*, 448, 521